2020 IEEE/RSJ International Conference on Intelligent Robots and Systems (IROS)
October 25-29, 2020, Las Vegas, NV, USA (Virtual)

An untethered soft cellular robot with variable volume, friction, and unit-to-unit cohesion

Matthew R. Devlin[1*], Brad T. Young[2], Nicholas D. Naclerio[1], David A. Haggerty[1], and Elliot W. Hawkes[1]

***Abstract*— A fundamental challenge in the field of modular and collective robots is balancing the trade-off between unit-level simplicity, which allows scalability, and unit-level functionality, which allows meaningful behaviors of the collective. At the same time, a challenge in the field of soft robotics is creating untethered systems, especially at a large scale with many controlled degrees of freedom (DOF). As a contribution toward addressing these challenges, here we present an untethered, soft cellular robot unit. A single unit is simple and one DOF, yet can increase its volume by 8x and apply substantial forces to the environment, can modulate its surface friction, and can switch its unit-to-unit cohesion while agnostic to unit-to-unit orientation. As a soft robot, it is robust and can achieve untethered operation of its DOF. We present the design of the unit, a volumetric actuator with a perforated strain-limiting fabric skin embedded with magnets surrounding an elastomeric membrane, which in turn encompasses a low-cost micro-pump, battery, and control electronics. We model and test this unit and show simple demonstrations of three-unit configurations that lift, crawl, and perform plate manipulation. Our untethered, soft cellular robot unit lays the foundation for new robust soft robotic collectives that have the potential to apply human-scale forces to the world.**

I. Introduction

In the field of modular and collective robotics, there is a challenging trade-off between the simplicity of a single unit and its functionality. Very simple units are highly scalable, enabling large unit-number collectives, but with limited functionality, the tasks that a unit or collective can do are limited. Conversely, a highly complex single unit allows functionality, yet makes scaling to large numbers of units difficult. An example of this phenomenon is seen in a comparison between more complex robotic systems, such as CEBOT [1] or Polybot [2], versus simpler ones, such as Kilobot [3] or particle robots [4]. To compare two systems by their ability to act on their environment, the Polybot is able to generate large actuation forces on its environment, but this comes at the cost of unit complexity. For example, all interactions between units require precisely aligned faces, and a mechanically actuated locking mechanism. In contrast, the Kilobot has a simpler unit that can be mass-produced, but cannot significantly actuate upon its environment [2], [3].

In the field of soft robotics, a significant challenge is realizing untethered systems. This challenge is especially pronounced for high degree of freedom (DOF) pneumatic systems, which usually rely on external pressure sources and valving [5]. For example, the 100-DOF soft haptic display relied upon a vast and complex array of off-board valves, controlling the pressure from a large pressure source [6]. There have been attempts to reduce this complexity of tethered soft modular systems in work such as [7], but untethered realizations remain a challenge.

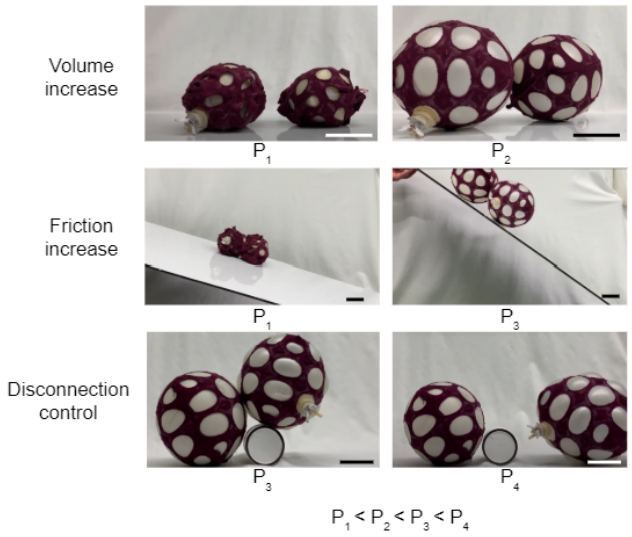

Fig. 1. Experimental demonstration of changing properties across a single inflation sequence. The first row demonstrates an increase in volume as pressure is increased from P_1 to P_2. The second row shows an increase in friction as pressure is increased to a higher level, P_3, visualized by the peak angle before slip. The third row demonstrates a controlled disconnection over an obstacle as the pressure is further increased from P_3 to P_4. Scale bar is 50 mm

In this work, we seek to contribute toward these two challenges in collective and soft robotics through the introduction of an untethered soft cellular robot unit (Fig. 1). This unit is simple to enable scalability yet able to vary its volume while applying significant forces to the environment, modulate its surface friction, and switch its unit-to-unit adhesion, connecting and disconnecting in an orientation-agnostic manner. At the same time, it is soft and robust to impact, yet untethered and if formed into a multi-unit collective, enables the simultaneous control many DOFs.

Soft, cellular, reconfigurable robots have not been explored deeply. Reference [8] reviews the state of the art of many soft modular robots, however few reconfigurable, soft robots have been developed. Many soft modular robots use magnets or electrostatic forces to allow unit-unit cohesion, such as

This work was supported in part by NSF Grant 1925373. The work of N. Naclerio was supported by a NASA Space Technology Research Fellowship.

[1]Department of Mechanical Engineering, University of California, Santa Barbara, CA 93106.

[2]College of Engineering, University of California, Santa Barbara, CA 93106.

* Corresponding author. Email: matthewdevlin@ucsb.edu

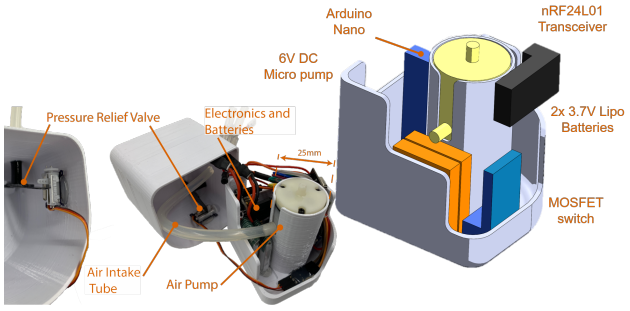

Fig. 2. The internal inflation unit of the robot wirelessly controls its inflation and deflation. A small diaphragm pump is used to inflate the robot, while a servo controlled pressure relief valve is used for deflation. A radio transmitter receives signals and a battery powers both.

in [9], [10], [11], [12], and soft actuators to disconnect the magnets [13]. While most shape change is from soft actuators, some use deformable metal strips to change shape [14]. Tunable friction methods to aid in locomotion have also been explored, leveraging anisotropic friction to enable locomotion or varied grasping [15], [16], however these systems are planar and have not been demonstrated in 3D configurations. The synthesis of a singular actuation mechanism to achieve both tunable friction and then disconnection is unique to this work.

In this paper, we first describe the design concept of our untethered soft cellular robot that enables the properties of variable volume, friction, and unit-to-unit adhesion, all with a single DOF input. We then present simple analytical models that describe the behavior of the unit, and perform several experiments to characterize the behavior of a unit. We then present a proof-of-concept prototype unit, with an inner electronics assembly to enable remote inflation and deflation (Fig. 2) and an outer skin of rayon fabric with embedded magnets, Eco-flex 00-30 silicone, and a latex membrane (Fig. 3). We then demonstrate how individual and small collectives behave.

II. Design Concept

In this section, we will briefly describe how the design of the unit allows it to control its volume, friction, and orientation-agnostic cohesion through a single degree of freedom (Fig. 1), while at the same time being untethered and soft with the ability to apply large forces.

The unit has a single DOF (internal pressure), which in turn regulates its volume, friction, and cohesion. Each unit is composed of a micro-pump inside of an elastomeric membrane, in turn surrounded by a strain-limiting layer perforated with holes. At low pressures, the elastomeric membrane is fully encapsulated by the low-friction strain-limiting layer, and changing pressure can control volume. At higher pressures, the strain-limiting layer is stretched taut, and the high-friction elastomeric membrane protrudes through the holes spread regularly in the fabric. This enables control of the unit's friction coefficient. This concept for friction control builds on previous work using both passive [16], [17] and active [15] variable friction mechanisms.

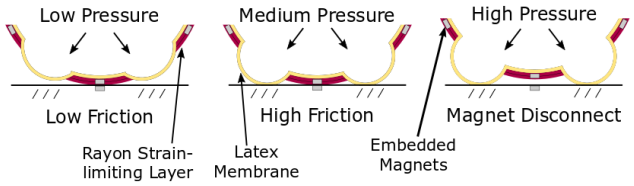

Fig. 3. Cross sectional representation of the robot layers. The latex inner layer is in yellow, the strain-limiting rayon layer in maroon, and the magnet in grey. As pressure increases, the inner layer protrudes through the strain limiting layer, increasing friction. As pressure increases further, the protrusions cause the magnet to disconnect.

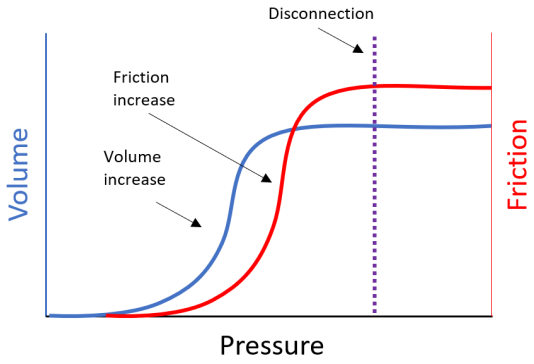

Fig. 4. Graphical representation of the relationship between pressure and volume, friction, and cohesion of a unit. As pressure increases, the unit will first undergo expansion. At a higher pressure, the protrusions bulge and the friction increases dramatically. Finally, when the protrusions are large enough, the magnets will disconnect. Note that the units are arbitrary, and the shapes of the curves are for illustrative purpose only.

The outer, strain-limiting layer contains regularly spaced magnets for unit-unit cohesion, with each magnet free to rotate. This design makes the units orientation agnostic and able to magnetically attach to each other in any orientation or configuration. The magnets negate the need for complex unit coupling mechanisms or awareness of another unit's position to connect. At pressures higher than those required for friction increase, the elastomeric membrane protrudes further, applying a rejection force between units. At a high enough pressure, this force overcomes the magnetic attraction, and the units separate. Thus, as pressure increases from zero, we first will see control of volume, then friction, and finally cohesion (Fig. 4).

Our soft cellular robots are untethered, uncommon in the field of soft robotics, allowing them to operate independently while still applying human scale forces on their environment. Each of the unit's pumps are powered by a battery, and controlled wirelessly. Although the units can only inflate to about 20 kPa, given the designed cross-sectional area of roughly 400 cm^2, two of them together can lift over 50 kg.

III. Single-unit Modeling

In this section, we present simple analytical models to help describe the basic trends of the behavior of the system. First, we describe the non-linear relationship between volume

and pressure, next between friction and pressure, and finally between cohesion and pressure.

A. Tunable volume

To model the relationship between the pressure inside a unit and its volume, we begin with a standard model of an inflating spherical elastic membrane before considering the effect of the strain limiting layer. The unconstrained model was derived using the approach from [18] and can be written as:

$$P = K\left(2\ln\frac{r}{r_0}\right)^n\left(\frac{t_0}{r}\right)\left(\frac{r_0}{r}\right)^3 \tag{1}$$

where P is the internal pressure, K is the strength coefficient, t_0 is the initial thickness of the material, r is radius of the unit, r_0 is the initial radius, and n is the material strain hardening exponent. To incorporate the effect of the strain-limiting layer, we assume a strain limit of ε_{max} and write the maximum radius, r_{max}, as:

$$r_{max} = \frac{\varepsilon_{max}}{2\pi r_0} + r_0. \tag{2}$$

Further, we note that the strain-limiting layer is compliant before reaching its strain limit. Thus, it effectively increases the modulus of the elastomeric membrane.

B. Tunable friction

In order to describe the tunable friction property of a unit, we wish to relate unit friction to the internal pressure. This is done by determining how the height of a protrusion of the membrane through the strain-limiting layer affects friction, then determining how pressure affects the height of the protrusion. As long as the height of the protrusions is less than the thickness of the strain-limiting layer, the friction will be determined by the properties of the strain-limiting layer. However, once the protrusion reaches a height that is greater than the strain-limiting layer, the friction will be set by the properties of the protrusion (see Fig. 3).

Next, to determine how pressure affects the height of the protrusion of the membrane through holes in the strain-limiting layer, we note that we have a case that is similar to the classic clamped circular inflated membrane problem. While others have suggested that Kirchoff thin-plate theory could be used to describe this system [15], such a model is inappropriate given the expected strains–Kirchoff only holds for small deflections, less than the thickness of the plate [19]. More appropriate is membrane theory, but no analytical solution can cover from small to large strain. Accordingly, we use an analytical approximation, created using the Galerkin method [20]. The approximation is:

$$\begin{aligned}\frac{P}{E} = \frac{1}{21(1-\nu^2)}\Bigg[&(46+28\nu-18\nu^2)\left(\frac{\delta_0}{a}\right)^2 \\ &+112\left(\frac{t}{a}\right)^2+84\varepsilon_0(1+\nu)\Bigg]\left(\frac{\delta_0}{a}\right)\left(\frac{t}{a}\right)\end{aligned} \tag{3}$$

where P is the internal pressure, E is the Young's modulus, ν is the Poisson's ratio, t is the material thickness, a is the hole radius, δ_0 is the vertical displacement, and ε_0 is the material prestrain. This analytical model was verified in [20] with experimental data. However, our system is more complex than the system modeled by (3), for at least two reasons. First, the diameter of the hole (in the the strain-limiting layer) increases with pressure until the strain-limiting layer reaches its non-stretch regime. Unlike silicone embedded fabric composites [21], [22], the elastic membrane is able to slide with respect to the strain-limiting layer which means that more elastic material than what is exposed within the hole can stretch and lead to increasing the height of the bulge. In essence, the radius is functionally larger. Modeling these effects are outside of the scope of this paper, and these models are used to inform design rather than be fully predictive. In particular, the general trends of (3) for thin membranes where $t/a << 1$ and moderate deflections where $\delta_0/a << 1$, (3) apply and simplify to:

$$\frac{P}{E} = \frac{4\varepsilon_o}{(1-\nu)}\frac{t}{a}\frac{\delta_0}{a}. \tag{4}$$

Notably, the pressure and the height of the protrusion are linearly related.

C. Tunable Cohesion

Lastly, to describe the robot's tunable cohesion, we assume that the units will disconnect once the separation force from inflation exceeds their magnetic cohesion force. We consider a simplified system that comprises two protrusions with a magnet between, as shown in Fig. 5. By symmetry, instead of modeling the second unit, we consider a flat plate with its own magnet. We assume that the separation force between the unit and plate is a sum of the force from the inflating protrusions, F_p, and any external forces, F_e, such as gravitational forces or friction acting on the unit. Disconnection occurs when the separation force overcomes the magnetic force, F_m, which can be written as:

$$\sum_i^n F_{p_i} + F_e > F_m, \text{ where } F_m = \frac{\mu_a q^2}{4\pi r^2}, \tag{5}$$

and r is the separation between magnets, q is their magnetic charge, and μ_a is the permeability of air [23]. Thus, for a known magnetic attraction force and characterized relationship between pressure and rejection force, the pressure at which disconnection occurs can be predicted (see Section IV-C).

IV. Experimental Testing of Tunable Properties

In this section, we provide experimental characterization of the three tunable properties of the unit described in Section III, namely, volume, friction, and cohesion, all as functions of pressure.

A. Tunable volume

To characterize the relationship between unit volume and pressure, we measured the diameter of a tethered unit at various pressures, both with and without the strain-limiting layer. Pressure was recorded by a pressure gauge (100PSI SSI Technologies, 0.25% accuracy), attached to the unit with

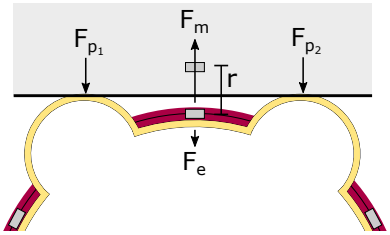

Fig. 5. Illustration of the forces at play for tunable unit-to-unit cohesion. Here we assume a flat plate on one side, due to a symmetry argument. Disconnection occurs when the sum of the force applied by the protrusions, F_p, and other external forces, F_e, is greater than the attractive force of the magnets, F_m. The elastomeric membrane is in yellow, the strain limiting layer in maroon, and the magnets in grey.

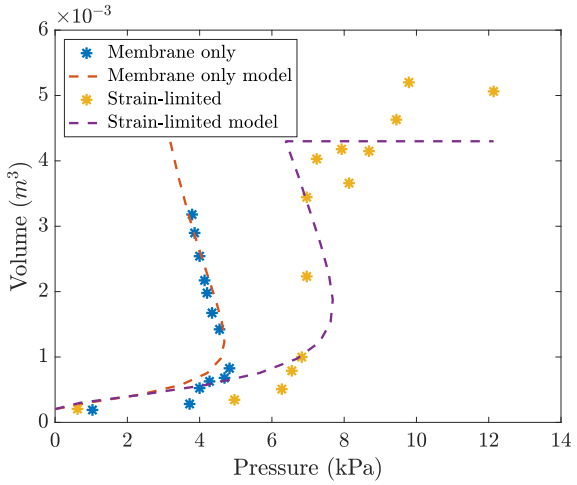

Fig. 6. Data showing the relationship between pressure and volume for an elastic membrane without constraint and an elastic membrane surrounded by a strain-limiting layer. Also shown are the models from Section III-A.

tubing. Radius was measured by image processing of a video of the inflating balloon with a known length reference. The balloon was assumed to be spherical to calculate volume from the measure radius. The results are shown in Fig. 6, along with the simple model from Section III-A, with K and n as fit parameters. The model captures the sharp increase in volume at a sufficient pressure for both with and without the strain-limiting layer. For the latter case, the model generally agrees with the trend of a plateauing volume at high pressures, however the assumption that the strain-limiting layer reaches a maximum strain and can no longer stretch is an oversimplification.

B. Tunable Friction

To characterize the tunable friction of a single unit, we first measured the frictional properties of its membrane materials, then characterized the height of a protrusion as a function of pressure, and finally measured the frictional force as a function of pressure.

The coefficient of friction of the Eco-flex 00-30 silicone (Smooth-On), latex (Gausslee Balloons), and rayon fabric (Telio) of the unit were measured using a drag test. Samples

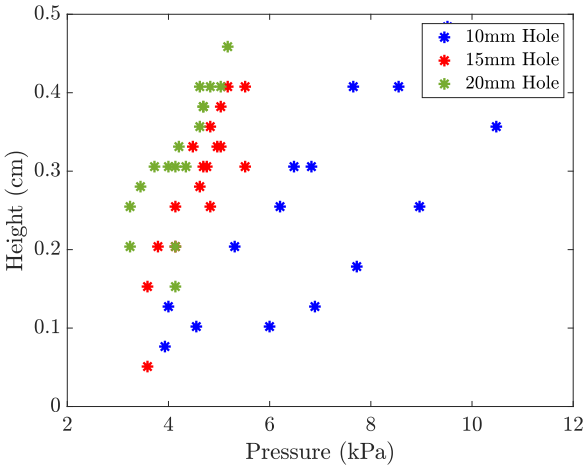

Fig. 7. Protrusion height versus pressure. Across a range of initial hole sizes, the protrusion height as a function of pressure is assessed for behavior characterization.

of 20mm x 50mm were placed on a flat, acrylic surface with four masses of various weight placed on top of them. The shear force required to cause slippage was measured by a Mark-10 M3-5 force gauge. The average coefficients of friction were found to be 1.6, 1.2, and 0.18 for Eco-flex 00-30, latex, and rayon respectively.

Next, we characterized the height of the latex balloon as a function of pressure as it protruded through a strain limiting layer with nominal hole sizes of 10mm, 15mm, and 20mm diameters. Hole sizes were selected to span the range of feasible sizes. If the protrusion hole sizes are too small (less than 10mm), the pressure required for balloon protrusion is greater than the strength of the seams of the fabric layer. If the protrusion hole sizes are too large (greater than 20mm), fabric bridges between holes tear under the stresses exerted by the protrusions. Protrusion height in an inflated unit was measured from the center of the protrusion to the base of the hole with calipers as pressure was increased. The experiment was run in triplicate for each hole size with the results plotted in Fig. 7, showing that protrusion height increases roughly linearly with pressure, as predicted by (4).

Finally, we characterized unit friction as a function of pressure. A drag test was performed on a unit with strain limiting layers with holes of 10mm, 15mm, and 20mm diameter. In each test, a flat, 200g acrylic plate was placed on top of a unit of various inflation pressures. The shear force required to slip the plate was measured with a Mark-10 M3-5 force gauge and used to calculate the coefficient of friction (μ). Three trials were conducted for each hole size with the result presented in Fig. 8. We show that μ approximately triples as the pressure increases. The friction transition can be predicted from the protrusion height data shown in Fig. 7. A height of roughly 6mm is required to expand the high-friction protrusion sufficiently beyond the low-friction strain-limiting layer. Thus, from Fig. 7, we would expect friction transitions at roughly 4kPa, 5kPa, and 8kPa for the 20mm, 15mm, and 10mm initial hole sizes, respectively.

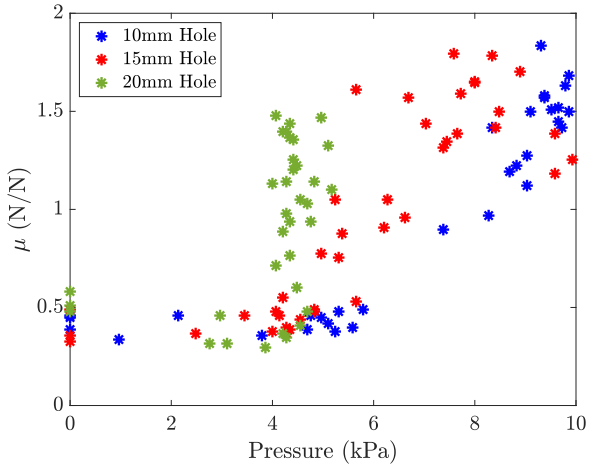

Fig. 8. Data showing the relationship between the pressure and the coefficient of friction (μ) for units with latex membranes and fabric strain-limiting layers. Three sizes of holes in the strain-limiting layer were tested.

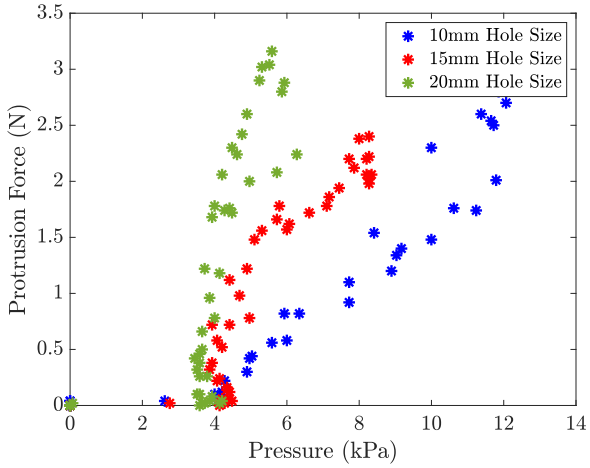

Fig. 9. Data showing the relationship between pressure and the rejection force applied by protrusions for various hole sizes.

C. Tunable cohesion

To characterize the relationship between cohesion and pressure, we first measured the rejection force of the protrusions as a function of pressure, and then recorded cohesion (connection or disconnection) as a function of pressure.

The rejection force of the protrusions was measured by recording their reaction force against a flat plate. A unit was placed against a flat plate and a force sensor (Mark 10 M3-5) was attached between two protrusions, as in where the magnet is pictured in Fig. 3. As the pressure of the unit was slowly increased, the protrusions pressed against the plate, applying a force to the sensor. The results are plotted in Fig. 9, showing that force increases as pressure, and therefore protrusion height, increases. They also show that larger hole sizes cause a larger protrusion force for a given pressure due to their increased height and area of protrusion.

Next, we measured unit cohesion as a function of pressure

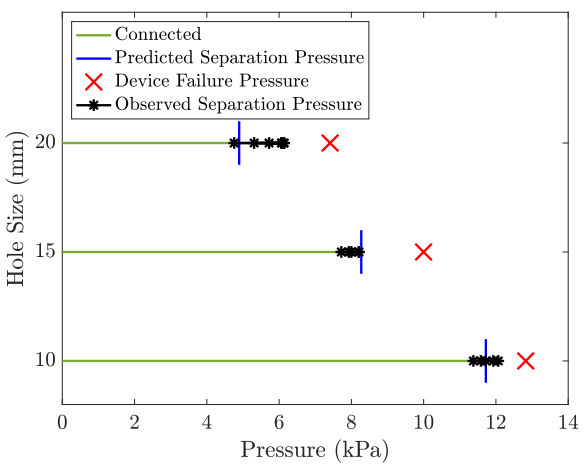

Fig. 10. Data showing the relationship between pressure and disconnection across multiple hole sizes, along with predicted disconnection pressure.

for the three hole sizes. The 40g latex membrane and fabric strain-limiting combination was hung from a magnetic plate, and pressure was slowly increased until disconnection, recorded in Fig. 10. As described in Section III-C, we can use the rejection force of the protrusions from Fig. 9, along with the predicted magnetic attraction force (here 2.5N for a 6 mm long, 3 mm in diameter cylindrical neodymium magnet) and external load (here 2.5N) to predict the disconnection pressure (blue vertical lines in Fig. 10).

V. Proof-of-Concept Robot

A. Design and Fabrication of an Untethered Unit

To demonstrate the soft cellular robot, we fabricated several untethered units of identical construction.

The body of the robot consists of an inner sealed elastic membrane and an outer, strain-limiting layer. The inner elastic membrane is made of a 0.35 mm thick latex rubber balloon, with a rated inflated diameter of 45 cm. To increase friction, the balloon is coated with a 0.5 mm thick layer of Eco-flex 00-30 silicone to increase the coefficient of friction beyond that available from latex alone. The outer strain limiting layer is made of two layers of four-way stretch rayon fabric. The fabric has 15 mm diameter holes spaced 30 mm apart in a regular grid throughout the fabric to allow the latex balloon to bulge out and form protrusions. Embedded in the fabric, between the two layers, are 6 mm long 3 mm diameter cross-axis magnetized cylindrical neodymium magnets (K&J Magnetics) for inter-unit cohesion. The magnets are free to rotate within the fabric to avoid directional issues and allow the units to remain orientation agnostic. We developed a layer-based manufacturing method for fabricating the skins. We create components via laser machining (for strain-limiting layer) and casting (for Eco-flex 00-30 frictional layer). We then assemble these components with the magnets in 2D before inserting the balloon and inflating into 3D.

Inside the skin is the inflation unit, that comprises a wireless pump, battery, electronics, and release valve as

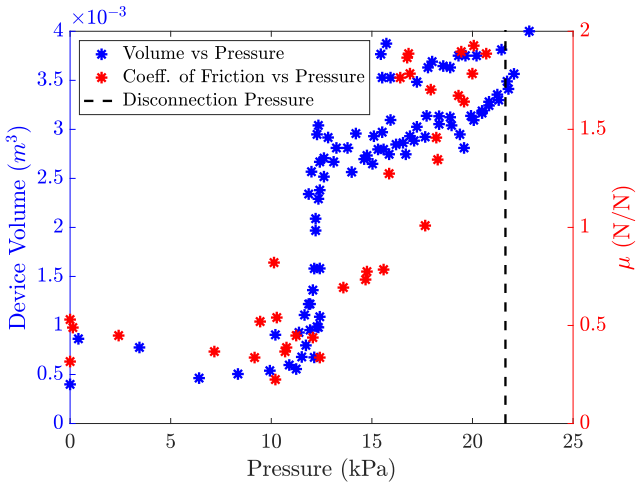

Fig. 11. Experimental characterization of volume, coefficient of friction, and disconnection as a function of pressure for a single prototype unit.

shown in Fig. 2. The pump is a 6V DC micro-diaphragm pump powered by two 3.7V, 250 mAh single cell lithium-ion batteries. Pressure is released by a custom 6mm diameter leaf valve actuated by a 2g linear throw servo motor. The inflation unit is able to pull and vent air from the environment through inlet and outlet tubing. Commands are sent wirelessly to the pump and valve by a NRF24L01 radio transmitter. The inflation electronics are contained within a 3D printed housing optimized for ease of insertion into the inner elastic membrane. The strain limiting layer is then stitched in place around the inflation unit and inner

B. Characterization of an Untethered Unit

We performed two tests to characterize the performance of a prototype unit, namely the effect of pressure on its tunable properties and its untethered inflation and deflation rate.

First, we characterized the relationship between the single input (pressure) and the three tunable properties (volume, friction, and cohesion) for an untethered unit. We wirelessly controlled the unit's internal pump to increase pressure to various levels while we recorded its volume, coefficient of friction, and pressure at which it disconnected from another unit. These results are shown in Fig. 11. Critically, the data shows that at low pressures, we can control volume, at intermediate pressures we can control its friction, and at the highest pressures, we can command disconnection.

Next, we characterized the time of inflation and deflation of the robot. The wireless micro-diaphragm pump inside the robot was capable of fully inflating the robot to disconnection pressure in 57 seconds, corresponding to a volume change of over 800%. After wirelessly opening the leaf valve, the unit deflated in 15 seconds.

C. Demonstration of Multi-cellular Robot

To illustrate very preliminary capabilities of multi-unit systems (here only three units), we performed demonstrations of lifting a heavy object, crawling, and plate manipulation.

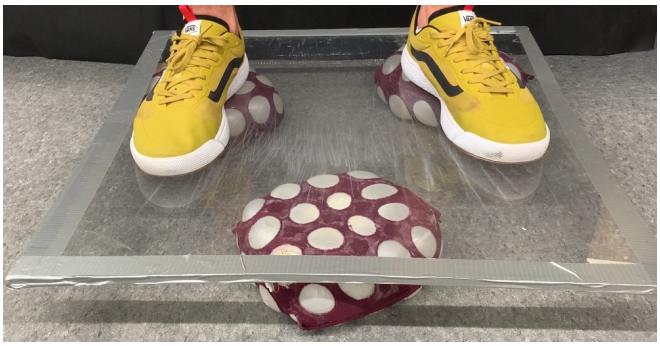

Fig. 12. Demonstration of three units supporting a 95 kg person.

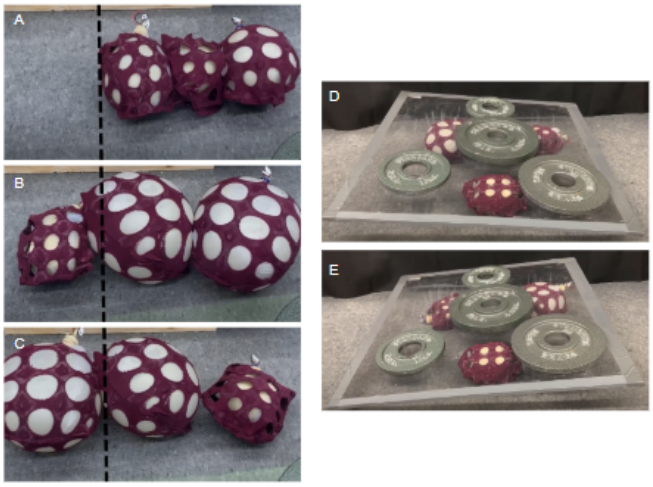

Fig. 13. A-C) A set of three units use a peristalic gait to crawl under an acrylic plate that is lower than their fully inflated height. D-E) Three units demonstrate manipulation of a 10 kg weighted plate as they vary their respective pressures.

First, we demonstrated the robot's lifting ability. Due to its inflation abilities, the untethered robot is capable of lifting heavy objects with its small internal electronics assembly. Three units were able to lift a 95 kg person, each exerting 310 N, as shown in Fig. 12. Each unit weighs only 248 g, therefore it can lift about 130x its own weight.

Second, we showed how the a robot consisting of three units can crawl using a peristaltic gait. A three-unit robot is placed between a weighted acrylic plate and the floor. This motion is shown in Fig. 13, A-C. In Fig. 13, D-E, a group of three units place underneath a 10 kg plate can manipulate the angle of the plate by controlling their relative pressure levels.

VI. Conclusions and Future Work

This work reports a first proof-of-concept of a single unit with tunable volume, friction, and cohesion that could become the building block of a multi-cellular robotic collective. We have demonstrated understanding and control over the protrusion height which is the primary mechanism for friction change and magnetic disconnection. In addition to the tunable properties, the unit showed large actuation forces

that are uncommon in an untethered, soft robotic system. We also developed a scalable layer-based manufacturing method for the skins of these units.

Looking to the future, we will undertake single unit optimization as well as begin to explore multi-unit behaviors and control. For unit optimization, the surface hole size and membrane thickness both have exponential impact on protrusion height, which dictates friction and disconnection. A key next step is advancing our models to more precisely predict behavior, rather than just trends. More thorough friction control characterization is also required to understand how this robot can operate in a variety of other environments such as on smooth laminate flooring or asphalt. Optimization can be tuned to application, for example, an increase in membrane thickness will decrease protrusion height sensitivity, but will increase the lifting potential of a single unit. In addition to tuning the exterior of the units, the electronics will include more sensing capabilities or some closed-loop control. For multi-unit systems, we are excited by the possibilities. From a control perspective, the limitation of central control could be overcome with distributed computing and simple sensor implementation. The potential with a distributed actuation system is also interesting, for example, only a 40 unit swarm could lift a 1000 kg car, which would be a first for soft robotic actuation. We also imagine that these units could enable interesting large-scale granule physics experiments with tunable particle friction and cohesion.

REFERENCES

[1] T. Fukuda and Y. Kawauchi, "Cellular robotic system (cebot) as one of the realization of self-organizing intelligent universal manipulator," in *Proceedings., IEEE International Conference on Robotics and Automation*. IEEE, 1990, pp. 662–667.

[2] D. Duff, M. Yim, and K. Roufas, "Evolution of polybot: A modular reconfigurable robot," in *Proc. of the Harmonic Drive Intl. Symposium, Nagano, Japan*, 2001.

[3] M. Rubenstein, C. Ahler, and R. Nagpal, "Kilobot: A low cost scalable robot system for collective behaviors," in *2012 IEEE International Conference on Robotics and Automation*, May 2012, pp. 3293–3298, iSSN: 1050-4729.

[4] S. Li, R. Batra, D. Brown, H.-D. Chang, N. Ranganathan, C. Hoberman, D. Rus, and H. Lipson, "Particle robotics based on statistical mechanics of loosely coupled components," *Nature*, vol. 567, no. 7748, pp. 361–365, Mar. 2019, number: 7748 Publisher: Nature Publishing Group. [Online]. Available: https://www.nature.com/articles/s41586-019-1022-9

[5] D. Rus and M. T. Tolley, "Design, fabrication and control of soft robots," *Nature*, vol. 521, no. 7553, pp. 467–475, May 2015. [Online]. Available: http://www.nature.com/articles/nature14543

[6] A. A. Stanley, "Haptic jamming: Controllable mechanical properties in a shape-changing user interface," Ph.D. dissertation, Stanford University, 2016.

[7] J.-Y. Lee, W. Kim, W.-Y. Choi, and K.-J. Cho, "Soft Robotic Blocks: Introducing SoBL, a Fast-Build Modularized Design Block," *IEEE Robotics & Automation Magazine*, vol. 23, pp. 1–1, Sept. 2016.

[8] C. Zhang, P. Zhu, Y. Lin, Z. Jiao, and J. Zou, "A review of modular soft robotics: Modular units, connection mechanisms, and applications," *Advanced Intelligent Systems*, p. 1900166, 2020.

[9] J. Zou, Y. Lin, C. Ji, and H. Yang, "A reconfigurable omnidirectional soft robot based on caterpillar locomotion," *Soft robotics*, vol. 5, no. 2, pp. 164–174, 2018.

[10] A. Vergara, Y.-s. Lau, R.-F. Mendoza-Garcia, and J. C. Zagal, "Soft Modular Robotic Cubes: Toward Replicating Morphogenetic Movements of the Embryo," *PLOS ONE*, vol. 12, no. 1, p. e0169179, Jan. 2017, publisher: Public Library of Science.

[11] S. Yim and M. Sitti, "SoftCubes: Stretchable and self-assembling three-dimensional soft modular matter:," *The International Journal of Robotics Research*, May 2014, publisher: SAGE PublicationsSage UK: London, England.

[12] J. Germann, M. Dommer, R. Pericet-Camara, and D. Floreano, "Active Connection Mechanism for Soft Modular Robots," *Advanced Robotics*, vol. 26, no. 7, pp. 785–798, Jan. 2012.

[13] S. W. Kwok, S. A. Morin, B. Mosadegh, J.-H. So, R. F. Shepherd, R. V. Martinez, B. Smith, F. C. Simeone, A. A. Stokes, and G. M. Whitesides, "Magnetic Assembly of Soft Robots with Hard Components," *Advanced Functional Materials*, vol. 24, no. 15, pp. 2180–2187, 2014.

[14] J. Lipton, L. Chin, J. Miske, and D. Rus, "Modular volumetric actuators using motorized auxetics," in *2019 IEEE/RSJ International Conference on Intelligent Robots and Systems (IROS)*. IEEE, 2019, pp. 7460–7466.

[15] K. P. Becker, N. W. Bartlett, M. J. D. Malley, P. M. Kjeer, and R. J. Wood, "Tunable friction through constrained inflation of an elastomeric membrane," in *2017 IEEE International Conference on Robotics and Automation (ICRA)*, May 2017, pp. 4352–4357, iSSN: null.

[16] A. Evora, E. Sloan, S. Castellino, E. W. Hawkes, and T. Susko, "Pilot Study of Cadence, a Novel Shoe for Patients with Foot Drop," in *2019 41st Annual International Conference of the IEEE Engineering in Medicine and Biology Society (EMBC)*. Berlin, Germany: IEEE, July 2019, pp. 5291–5296.

[17] S. A. Suresh, C. F. Kerst, M. R. Cutkosky, and E. W. Hawkes, "Spatially variant microstructured adhesive with one-way friction," *Journal of The Royal Society Interface*, vol. 16, no. 150, p. 20180705, Jan. 2019.

[18] M. M. Carroll, "Radial expansion of hollow spheres of elastic-plastic hardening material," *International Journal of Solids and Structures*, vol. 21, no. 7, pp. 645–670, jan 1985.

[19] E. Ventsel, T. Krauthammer, and E. Carrera, "Thin plates and shells: theory, analysis, and applications," *Appl. Mech. Rev.*, vol. 55, no. 4, pp. B72–B73, 2002.

[20] Q. Yang, P. Kobrin, C. Seabury, S. Narayanaswamy, and W. Christian, "Mechanical modeling of fluid-driven polymer lenses," *Applied Optics*, vol. 47, no. 20, pp. 3658–3668, July 2008, publisher: Optical Society of America.

[21] Y. Wang and M. A. Minor, "Design and Evaluation of a Soft Robotic Smart Shoe for Haptic Terrain Rendering," *IEEE/ASME Transactions on Mechatronics*, vol. 23, no. 6, pp. 2974–2979, dec 2018.

[22] Y. Wang, C. Gregory, and M. A. Minor, "Improving mechanical properties of molded silicone rubber for soft robotics through fabric compositing," *Soft Robotics*, vol. 5, no. 3, pp. 272–290, jun 2018. [Online]. Available: https://www.liebertpub.com/doi/10.1089/soro.2017.0035

[23] A. T. Borges and J. K. Gilbert*, "Models of magnetism," *International Journal of Science Education*, vol. 20, no. 3, pp. 361–378, Mar. 1998.